Spin-isomer conversion of water at room temperature, and quantum-rotor-induced nuclear polarization, in the water-endofullerene $H_2O@C_{60}$

Benno Meier,* Karel Kouřil,† Christian Bengs, Hana Kouřilová, Timothy C. Barker, Stuart J. Elliott, Shamim Alom, Richard J. Whitby, and Malcolm H. Levitt‡
School of Chemistry, University of Southampton, Southampton, SO17 1BJ, United Kingdom
(Dated: June 1, 2018)

Water exists in two forms, *para* and *ortho*, that have nuclear spin states with different symmetries. Here we report the conversion of fullerene-encapsulated *para*-water to *ortho*-water. The enrichment of *para*-water at low temperatures is monitored via changes in the electrical polarizability of the material. Upon rapid dissolution of the material in toluene the excess *para*-water converts to *ortho*-water. In $H_2{}^{16}O@C_{60}$ the conversion leads to a slow increase in the NMR signal. In $H_2{}^{17}O@C_{60}$ the conversion gives rise to weak signal enhancements attributed to quantum-rotor-induced nuclear spin polarization. The time constants for the *para*-to-*ortho* conversion of fullerene-encapsulated water in ambient temperature solution are estimated as 30±4 s for the ^{16}O-isotopologue of water, and 16±3 s for the ^{17}O isotopologue.

The wavefunction of a water molecule is antisymmetric under exchange of its two protons, and may be written as a product of a rotational state and a nuclear spin state. Two different spin isomers of water exist: In *para*-water the rotational state is symmetric, with an antisymmectric nuclear spin state with total spin $I = 0$. In *ortho*-water the rotational state is antisymmetric, and the nuclear spin state is one of the three symmetric triplet states, with total spin $I = 1$. The rotational ground-states of free *para* and *ortho*-water have $J = 0$ and $J = 1$, respectively, and exhibit a splitting of 34 K [1].

The ratio of water spin isomers has been used to estimate the formation temperature of water in astrophysics [2, 3]. Differences in the magnetic and electric properties have been used to separate the spin isomers in molecular beam experiments [4, 5]. The conversion of water between its spin isomers has been followed at low temperatures by infrared spectroscopy [6, 7] in inert gas matrices. A remarkable lifetime of 26 minutes has been claimed for bulk *para*-water under ambient conditions [8], although this claim has been disputed [9, 10].

The molecular endofullerene $H_2O@C_{60}$, produced by multi-step chemical synthesis [11, 12], provides an excellent system for studying water spin isomers. Each C_{60} fullerene cage encapsulates a single water molecule which retains free molecular rotation at low temperatures [1, 13]. The cage prevents the exchange of protons between water molecules, which provides a mechanism for rapid *ortho-para* equilibration in bulk water [14]. Spin-isomer conversion in water endofullerenes has been studied by infrared spectroscopy, neutron scattering, NMR, and via changes in dielectric constant [1, 13, 15, 16]. The conversion of *ortho-* to *para*-water follows second order kinetics, indicating that it is facilitated by water-water interactions that may involve the electric dipole moments of neighbouring water molecules [15].

Here we report on the conversion between *para* and *ortho* water spin isomers in the endofullerene $H_2O@C_{60}$, in room-temperature solution. Alongside the spin-isomer conversion, we also observe weak nuclear spin polarization effects for water molecules bearing a ^{17}O nucleus. These quantum-rotor-induced polarization (QRIP) effects are related to analogous effects observed in unhindered ^{13}C-bearing methyl (CH_3) rotors [17–19].

The ^{1}H NMR spectrum of $H_2O@C_{60}$, with a ^{17}O labelling level of 85 % and dissolved in deuterated ortho-dichlorobenzene (ODCB), is shown in Fig. 1. The ^{1}H NMR spectrum exhibits 6 peaks due to the J-coupling of the two equivalent protons to the spin-5/2 ^{17}O nu-

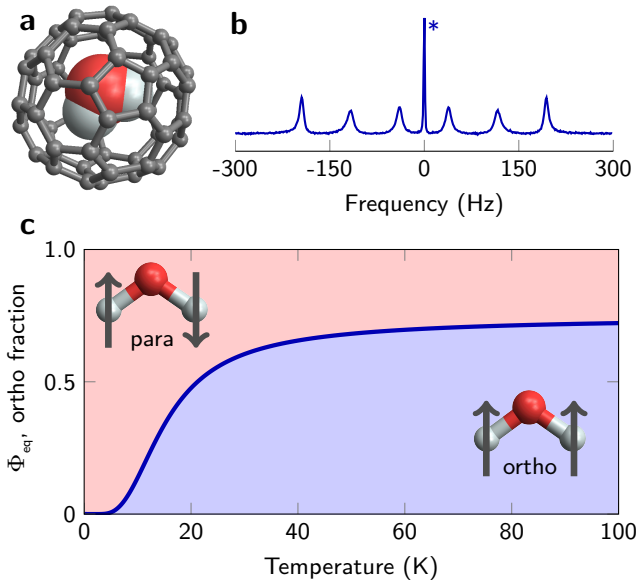

FIG. 1. (a) Molecular structure of $H_2O@C_{60}$. (b) ^{1}H NMR spectrum of $H_2O@C_{60}$, with a ^{17}O labelling level of 85 %, dissolved in deuterated ortho-dichlorobenzene. The proton resonance is split into a sextet due to the J-coupling to the spin-5/2 oxygen. The central line is due to the 15% of water bearing the ^{16}O isotope. (c) Equilibrium *ortho*-fraction as a function of temperature. At high temperatures, 75% of the molecules are in the *ortho* state. At 5 Kelvin and in thermal equilibrium, the *ortho*-state is almost completely depleted.

cleus. The linewidths of the ^{1}H NMR peaks are dominated by ^{17}O quadrupolar relaxation [20]. The sharp central peak is due to the 15 % of molecules bearing the ^{16}O isotope. At 25 °C the ^{1}H T_1 values were reported previously to be 700±50 ms for $H_2{}^{16}O@C_{60}$, and 750±50 ms for $H_2{}^{17}O@C_{60}$. The ^{17}O T_1 is 81 ± 7 ms [20].

The *ortho*-H_2O ground state in $H_2O@C_{60}$ is approximately 2.7 meV higher in energy than the *para*-H_2O ground state, as determined by neutron scattering [1]. Hence temperatures below ∼20 K strongly favour the *para*-H_2O state in thermal equilibrium. Fig. 1c shows the equilibrium proportions of *ortho* and *para*-H_2O as a function of temperature.

In the current work, we enhanced the fraction of *para*-H_2O by thermal equilibration at low temperature, and raised the temperature rapidly by dissolving the material in a warm solvent. The ^{1}H NMR spectrum was observed while *para*-water converts back to *ortho*-water at ambient temperature.

One experimental difficulty is that solid $H_2O@C_{60}$, just like C_{60}, dissolves only slowly, due to strong intermolecular interactions. Since slow dissolution is incompatible with observation of the rapid *para*-to-*ortho* conversion process, we first dissolved $H_2O@C_{60}$ in deuterated ODCB, at a concentration of 17 mM [21]. Dissolution proceeds rapidly when the frozen solid solution is exposed to warm solvent.

The kinetics of *ortho-para* conversion in pure $H_2O@C_{60}$ solid indicate that interactions between water molecules are important for the spin-isomer conversion process [15]. The use of a frozen solution generates uncertainty as to whether the water molecules in the frozen endofullerene solution do become enriched in the *para* spin isomer. The required pre-dissolution of $H_2O@C_{60}$ in ODCB increases the distance between water-molecules, and may change, and potentially suppress, the conversion to *para*-water.

To resolve this issue we studied the *ortho-para* conversion of $H_2{}^{16}O@C_{60}$ in frozen ODCB solution by measuring the dielectric constant of the material. The electric polarizability of *ortho*-water is larger than that of *para*-water, in their respective rotational ground-states. As water converts from *ortho*- to *para*-water, the dielectric constant decreases. The techniques and analysis are similar to those reported in Ref. [16]. A new dielectric probe was constructed that can be loaded with liquid samples. The probe comprises three nearly identical, cylindrical capacitors that were loaded with solutions of C_{60} in ODCB, $H_2{}^{16}O@C_{60}$ in ODCB, and $H_2{}^{17}O@C_{60}$ in ODCB respectively. The dielectric data show that spin conversion does occur, and lead to an estimated *para*-fraction of 0.4 after 28 h at 4.2 K. Details of the dielectric probe, the measurement and analysis are given in the SI.

In order to observe spin isomer conversion at ambient temperature, the sample is dissolved and the spectra are recorded using a liquid-state NMR apparatus. We

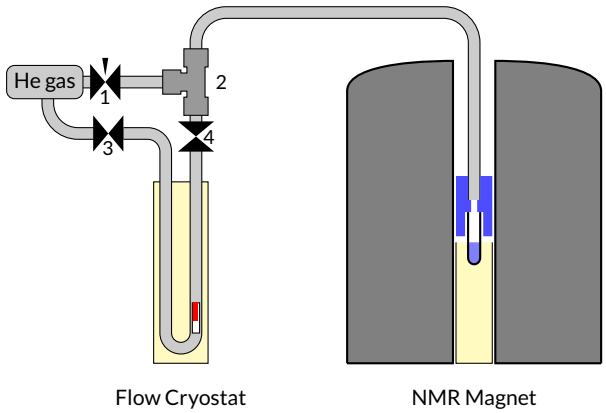

FIG. 2. Apparatus for rapid dissolution. Approximately 50 µL of sample (red) are pipetted into a teflon bullet which is then immersed in liquid nitrogen. For loading, the tube at the top of the union (2) is disconnected, the ball valve (4) is opened and the bullet is pushed to the bottom of the steel tube. A small flow of helium gas, applied via the needle valve (1), prevents contamination of the system with air. The capsule is ejected by opening valves (3) and (4) and is propelled into the NMR magnet (right), where a 3D printed receiver (blue) retains the capsule and vents the helium gas. The sample travels further into the 5 mm NMR tube where it dissolves in warm solvent.

rapidly dissolved the sample using a home-built penumatic shuttle, shown in Fig. 2. A 1/4" steel tube (Swagelok, UK) was bent into a U-shape, the ends were fed through a KF-50 brass blank (Kurt Lesker, UK), and the tubing was brazed to the blank. Manual ball valves (Swagelok) are used to open and close the tube on either end. A small flow of helium gas is applied via a needle valve (Swagelok), to prevent contamination of the system with air during loading and ejection. The transfer of the sample to the secondary magnet takes approximately 100 ms. A 3D printed receiver structure retains the sample capsule and vents the helium gas, but allows the sample to travel further into a 5 mm NMR tube preloaded with warm solvent. A detailed drawing of the receiver structure is provided in the SI. The shuttle enables dissolution with a much smaller solvent volume than previous procedures [22], with gains in concentration and sensitivity that are critical for the experiments described here. The shuttle is mounted in a commercial flow cryostat (Oxford Instruments), that is located, for an unrelated purpose, in a 6.7 Tesla magnet. The field has no significant effect on the *ortho*/*para* conversion, but leads to a magnetization of the *ortho*-water.

Separate experiments were conducted to study the *para*/*ortho* conversion of $H_2{}^{16}O@C_{60}$ and $H_2{}^{17}O@C_{60}$. In the first experiment a sample of 50 µL $H_2{}^{16}O@C_{60}$ in ODCB was kept at a temperature of 3.9 Kelvin for approximately 15 hours. ^{1}H NMR spectra were recorded every 1 s using a flip-angle of approximately 30°. Acquisition of NMR data was started approximately 20 s

before the sample was ejected from the cryostat and dissolved in the NMR tube. The obtained spectra were multiplied with a Lorentzian mask and integrated to obtain the NMR signal intensity, shown in Fig. 3.

The sharp peak in NMR signal immediately after dissolution is attributed to the nuclear magnetization of *ortho*-water which was pre-polarized by keeping the sample in a magnetic field at low temperatures. This peak decays rapidly with the proton T_1 of $\sim 0.8\,\mathrm{s}$. Subsequently the signal intensity slowly increases as *para*-water converts to *ortho*-water.

Results of an analogous experiment, conducted on $H_2{}^{17}O@C_{60}$, are shown in Fig. 4. For this experiment, the sample was kept at a temperature of 4 Kelvin for approximately 15 h. ^{1}H NMR spectra were recorded every 250 ms using a flip-angle of approximately 30°.

Figure 4(b) shows the evolution of the NMR spectrum after dissolution of the sample. Spectra were averaged over a total acquisition time of 5 seconds to improve the signal-to-noise ratio. Spectra averaged during the first 5 seconds clearly show an anti-phase pattern that is characteristic for QRIP [19, 23, 24]. The time-evolution of the individual peaks is obtained by multiplying the spectra with Lorentzian masks as shown in panel (c), followed by integration. The corresponding trajectories for the six $H_2{}^{17}O@C_{60}$ peaks, normalized by their respective thermal intensities and with a tri-cube bandwidth reduction of width 2 s, are shown in panel (d). The procedure is

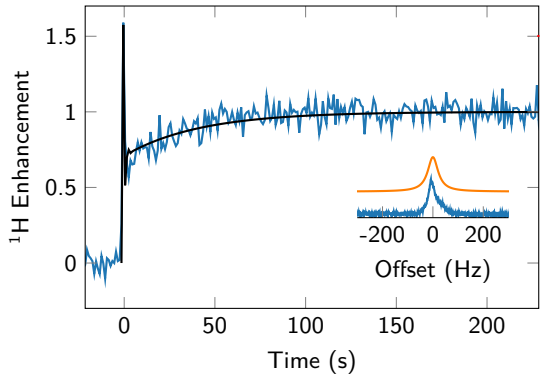

FIG. 3. Intensity of the ^{1}H NMR signal of $H_2{}^{16}O@C_{60}$ in solution as a function of time (blue curve). Acquisition starts prior to arrival of the sample. The time origin is chosen to coincide with the first NMR signal after dissolution of the sample. The initial sharp peak is due to initial *ortho*-water magnetization (the cryostat is located in a 6.7 Tesla magnet), and decays rapidly with the proton T_1. Following the rapid decay the signal intensity increases with time as *para*-water converts to *ortho*-water. The black curve shows the result of a spin dynamical simulation with a time constant $T_S = 30\,\mathrm{s}$ for the conversion of *para*-water to *ortho*-water (see text). The inset shows a spectrum (lower, blue curve) obtained from averaging 20 transients recorded 8 min after dissolution of the sample, and a Lorentzian mask (upper, orange curve) that was applied prior to integration.

detailed in the SI which includes Ref. [25]. Panels (e-j) show separate plots of the six peak intensities, together with trajectories obtained from spin dynamical simulations. The outermost peaks exhibit small enhancements of up to 2. A thermal equilibrium spectrum is shown in Fig. 4(a).

Simulations of the proton peak trajectories during the spin-isomer conversion process of both $H_2{}^{16}O@C_{60}$ and $H_2{}^{17}O@C_{60}$ were performed by using *SpinDynamica* software with a modified thermalization procedure (see below) [26–30]. The simulations for $H_2{}^{16}O$ included ^{1}H-^{1}H dipole relaxation and spin-rotation. In the case of $H_2{}^{17}O$, ^{1}H-^{17}O dipole-dipole relaxation, ^{17}O quadrupolar relaxation, and their cross-correlations were also included, along with the experimentally observed ^{1}H-^{17}O J-coupling of 77.9 Hz.

The relevant interactions were derived from the known molecular geometry and the ^{17}O quadrupole coupling constant of 10.11 MHz [31]. In order to match the experimentally observed relaxation time of 86 ms for the ^{17}O longitudinal magnetization, a rotational correlation time of $\tau_C = 107\,\mathrm{fs}$ was used for the simulation of both water isomers [20].

An external random field contribution, characterized by the magnitude of the random fields and correlation coefficients $\kappa_{i,j}$ [23], was included in order to model spin-rotation coupling. All relaxation processes were treated by using a relaxation superoperator in the isotropic fast-motion limit as detailed in Ref. [20]. A random field of $\eta_{\mathrm{H}}^{\mathrm{rand}^2}\tau^{\mathrm{rand}} = 0.6\ \mathrm{s}^{-1}$ was used to model spin-rotation relaxation in order to match the experimentally observed longitudinal relaxation time of 755 ms for the proton spins.

The time constant for the *para*/*ortho* equilibration is related to the rates for *para*-to-*ortho* conversion, $k_{p\to o}$ and the reverse process, $k_{o\to p}$, as follows:

$$T_S^{-1} = 4k_{p\to o} = \frac{4}{3}k_{o\to p}. \qquad (1)$$

The time constant for para-to-ortho conversion is denoted here T_S, since this quantity corresponds precisely to the decay time constant of singlet order, in the NMR of long-lived spin states [27–29]. The relaxation superoperator yields the following expressions for $k_{p\to o}$ for the two water isotopologues:

$$k_{p\to o}(H_2{}^{16}O) = \eta_{\mathrm{H}}^{\mathrm{rand}^2}\tau^{\mathrm{rand}}(1-\kappa) \qquad (2)$$

$$k_{p\to o}(H_2{}^{17}O) = k_{p\to o}(H_2{}^{16}O) + k_{\mathrm{DD}}^{\mathrm{OH}}. \qquad (3)$$

For ^{16}O, good agreement with experimental data is found for $T_S(H_2{}^{16}O) = 30 \pm 4\,\mathrm{s}$, corresponding to $\kappa = 0.986 \pm 0.002$ (black curve in Fig. 3).

In the case of $H_2{}^{17}O$, $k_{\mathrm{DD}}^{\mathrm{OH}}$ accounts for the additional contribution of the ^{1}H-^{17}O dipole-dipole interactions. A general expression has been given in Equation 4 of Ref. [32]. Here the couplings of the protons to the

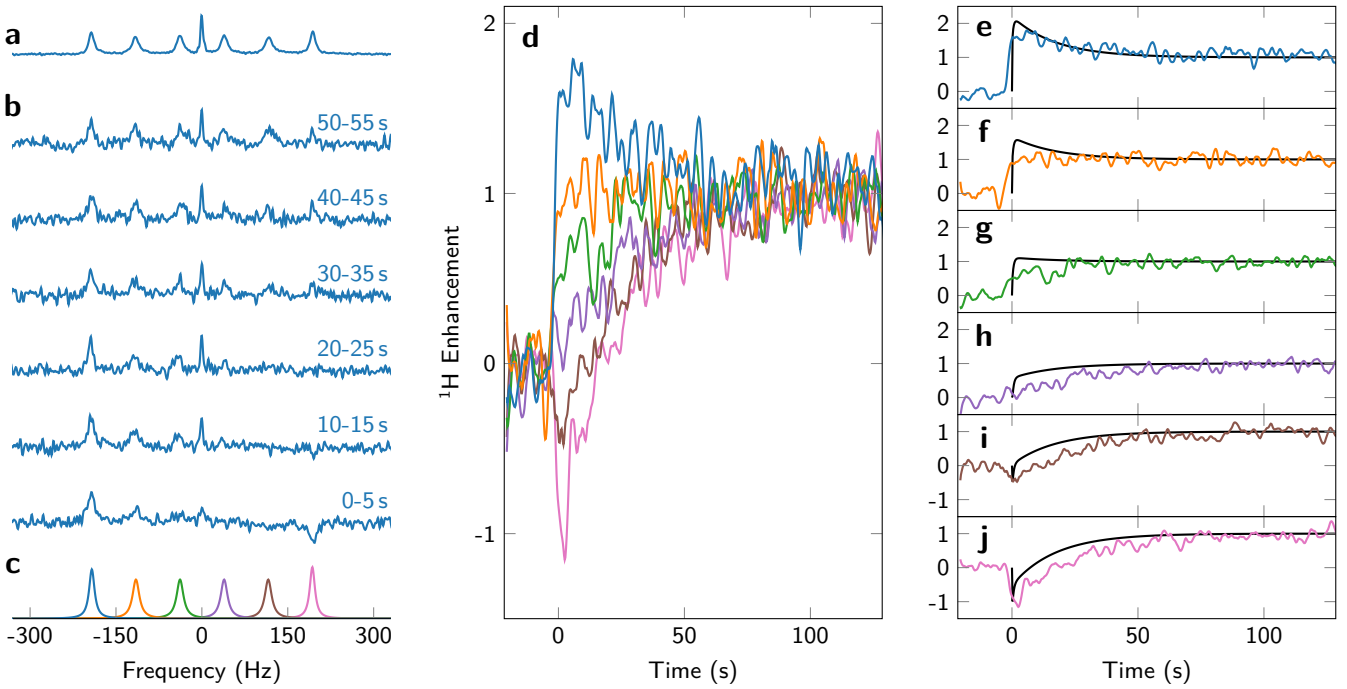

FIG. 4. QRIP Experiment on $H_2{}^{17}O@C_{60}$. (a) Thermal equilibrium ^{1}H spectrum, recorded after equilibration of the sample (1024 transients averaged). (b) Averages of 20 transients during consecutive intervals after dissolution of the sample. A clear antiphase signal is obtained immediately after the dissolution (0-5s). The antiphase signal decays, and after approximately one minute the thermal signal is restored. (c) The individual spectra are multiplied with Lorentzian masks that correspond to each of the six peaks, and the product is integrated. (d) Results of the integration after applying a tri-cube bandwidth reduction of width 2 s. The integrals are normalized by the intensity of the respective thermal ^{17}O peaks. (e-j) The same data as in (d), with spin dynamical simulations (black lines).

spin 5/2 heteronucleus are identical, and the expression simplifies to

$$k_{\mathrm{DD}}^{\mathrm{OH}} = \frac{35}{4}\left(\frac{\hbar\mu_0}{4\pi}\frac{\gamma^{17\mathrm{O}}\gamma^{1\mathrm{H}}}{r^3}\right)^2 \tau_C \sin^2\theta = 0.0087\,\mathrm{s}^{-1}, \quad (4)$$

where $\gamma^{17\mathrm{O}}$ and $\gamma^{1\mathrm{H}}$ are the gyromagnetic ratios of ^{17}O and ^{1}H, respectively, and τ_C is the correlation time, assumed to be $\tau_C = 107\,\mathrm{fs}$. The numeric result is obtained using the ^{1}H-^{17}O-distance r and and the H-O-H angle θ of the endohedral molecule from quantum chemistry calculations [33]. For $H_2{}^{17}O@C_{60}$ good agreement with experimental data is found for $\kappa \in [0.99, 1]$, corresponding to $T_S(H_2{}^{17}O) = 16 \pm 3\,\mathrm{s}$.

This analysis shows that the experimental data and theory may only be reconciled by assuming a very high degree of correlation for the random fields used to model the spin-rotation interaction. Numerical simulations indicate that contributions from quadrupolar relaxation have negligible influence on the *para/ortho*-conversion kinetics.

In NMR, the evolution of the spin density operator is typically described by the following master equation [34]:

$$\dot{\rho}(t) = -i\hat{\mathrm{H}}_{\mathrm{coh}}\rho(t) + \hat{\Gamma}(\rho(t) - \rho_{\mathrm{eq}}) \quad (5)$$

where $\hat{\mathrm{H}}_{\mathrm{coh}}$ is the commutation superoperator of the coherent Hamiltonian and ρ_{eq} the thermal equilibrium density operator. This equation is a good approximation for spin systems which are close to thermal equilibrium, but leads to incorrect results for spin systems that are far from equilibrium, which is the case here. The simulations shown in Figs. 3 and 4 made use of the homogeneous master equation [35, 36]:

$$\dot{\rho}(t) = -i\hat{\mathrm{H}}_{\mathrm{coh}}\rho(t) + \hat{\Gamma}_\theta(\rho(t)) \quad (6)$$

The thermally corrected relaxation superoperator $\hat{\Gamma}_\theta$ is given by:

$$\hat{\Gamma}_\theta = \hat{\Gamma}\exp\left(\hat{\mathrm{H}}_{\mathrm{lab}}^{\mathrm{L}}\hat{P}_D/(k_{\mathrm{B}}T)\right) \quad (7)$$

where $\hat{\mathrm{H}}_{\mathrm{lab}}^{\mathrm{L}}$ is the left translation superoperator [34] of the laboratory-frame coherent Hamiltonian $\mathrm{H}_{\mathrm{lab}}$ and $\hat{P}_D$ is the diagonal part projector with respect to the Hamiltonian $\mathrm{H}_{\mathrm{lab}}$ [37]. Unlike the forms proposed in Refs. [35, 36], this superoperator respects detailed balance [37] and provides physically reasonable results even for spin systems far from thermal equilibrium.

The density operator immediately after dissolution is determined by the initial fraction of *para*- and *ortho*-water. The initial fractions are not known a priori and were adjusted to give the best agreement between simulations and data. The simulation results are shown as

black curves in Fig. 3 and Fig. 4(e-j) for $H_2{}^{16}O@C_{60}$ and $H_2{}^{17}O@C_{60}$ respectively. The initial *para*-fractions are estimated as 54±15 % and 43±3 %, respectively, where the larger uncertainty for $H_2{}^{16}O@C_{60}$ is due to the smaller dynamic range of the $H_2{}^{16}O$ data.

In conclusion, NMR experiments were used to study the spin isomer conversion for the endohedral water molecules of $H_2O@C_{60}$ in ambient-temperature solution. The time constants for the *para*/*ortho* equilibration are found to be 30±4 s for the ^{16}O isotopologue of water, and 16±3 s for the ^{17}O isotopologue. The faster *para*-to-*ortho* conversion of $H_2{}^{17}O$ is attributed to ^1H-^{17}O dipole-dipole interactions. Weak nuclear spin polarization effects are observed for the ^{17}O isotopologue as the spin isomer conversion proceeds. Measurements of electrical capacitance at low temperature indicate that slow conversion between the water spin isomers also takes place in frozen solutions of $H_2O@C_{60}$ in ODCB, with the conversion again proceeding more rapidly for the ^{17}O isotopologue than for the ^{16}O species.

We acknowledge discussions with Walter Köckenberger and Sankeerth Hebbar. This research was supported by EPSRC (UK), grant codes EP/N002482, EP/M001962/1, EP/L505067/1, and EP/P009980 and the Wolfson Foundation.

* b.meier@soton.ac.uk
† B Meier and K Kouřil contributed equally.
‡ mhl@soton.ac.uk

[1] C. Beduz, M. Carravetta, J. Y.-C. Chen, M. Concistre, M. Denning, M. Frunzi, A. J. Horsewill, O. G. Johannessen, R. Lawler, X. Lei, and et al., Proceedings of the National Academy of Sciences **109**, 12894 (2012).
[2] T. Encrenaz, Annual Review of Astronomy and Astrophysics **46**, 57 (2008).
[3] M. R. Hogerheijde, E. A. Bergin, C. Brinch, L. I. Cleeves, J. K. J. Fogel, G. A. Blake, C. Dominik, D. C. Lis, G. Melnick, D. Neufeld, O. Panic, J. C. Pearson, L. Kristensen, U. A. Yildiz, and E. F. van Dishoeck, Science **334**, 338 (2011).
[4] T. Kravchuk, M. Reznikov, P. Tichonov, N. Avidor, Y. Meir, A. Bekkerman, and G. Alexandrowicz, Science **331**, 319 (2011).
[5] D. A. Horke, Y.-P. Chang, K. Długołęcki, and J. Küpper, Angewandte Chemie International Edition **53**, 11965 (2014).
[6] R. L. Redington and D. E. Milligan, The Journal of Chemical Physics **39**, 1276 (1963).
[7] P.-A. Turgeon, P. Ayotte, E. Lisitsin, Y. Meir, T. Kravchuk, and G. Alexandrowicz, Phys. Rev. A **86**, 062710 (2012).
[8] V. I. Tikhonov, Science **296**, 2363 (2002).
[9] P. Cacciani, J. Cosléou, and M. Khelkhal, Physical Review A **85**, 012521 (2012).
[10] S. L. Veber, E. G. Bagryanskaya, and P. L. Chapovsky, Journal of Experimental and Theoretical Physics **102**, 76 (2006).
[11] K. Kurotobi and Y. Murata, Science **333**, 613 (2011).
[12] A. Krachmalnicoff, M. H. Levitt, and R. J. Whitby, Chem. Commun. **50**, 13037 (2014).
[13] K. S. K. Goh, M. Jiménez-Ruiz, M. R. Johnson, S. Rols, J. Ollivier, M. S. Denning, S. Mamone, M. H. Levitt, X. Lei, Y. Li, N. J. Turro, Y. Murata, and A. J. Horsewill, Phys. Chem. Chem. Phys. **16**, 21330 (2014).
[14] D. Mammoli, N. Salvi, J. Milani, R. Buratto, A. Bornet, A. A. Sehgal, E. Canet, P. Pelupessy, D. Carnevale, S. Jannin, and G. Bodenhausen, Phys. Chem. Chem. Phys. **17**, 26819 (2015).
[15] S. Mamone, M. Concistrè, E. Carignani, B. Meier, A. Krachmalnicoff, O. G. Johannessen, X. Lei, Y. Li, M. Denning, M. Carravetta, K. Goh, A. J. Horsewill, R. J. Whitby, and M. H. Levitt, The Journal of Chemical Physics **140**, 194306 (2014).
[16] B. Meier, S. Mamone, M. Concistrè, J. Alonso-Valdesueiro, A. Krachmalnicoff, R. J. Whitby, and M. H. Levitt, Nature Communications **6**, 8112 (2015).
[17] M. Icker and S. Berger, Journal of Magnetic Resonance **219**, 1 (2012).
[18] M. Icker, P. Fricke, T. Grell, J. Hollenbach, H. Auer, and S. Berger, Magnetic Resonance in Chemistry **51**, 815 (2013).
[19] B. Meier, J.-N. Dumez, G. Stevanato, J. T. Hill-Cousins, S. S. Roy, P. Håkansson, S. Mamone, R. C. D. Brown, G. Pileio, and M. H. Levitt, J. Am. Chem. Soc. **135**, 18746 (2013).
[20] S. J. Elliott, C. Bengs, K. Kouril, B. Meier, S. Alom, R. J. Whitby, and M. H. Levitt, ChemPhysChem **19**, 251 (2018).
[21] N. O. Mchedlov-Petrossyan, Chemical Reviews **113**, 5149 (2013).
[22] J. H. Ardenkjaer-Larsen, B. Fridlund, A. Gram, G. Hansson, L. Hansson, M. H. Lerche, R. Servin, M. Thaning, and K. Golman, Proceedings of the National Academy of Sciences **100**, 10158 (2003).
[23] J.-N. Dumez, P. Håkansson, S. Mamone, B. Meier, G. Stevanato, J. T. Hill-Cousins, S. S. Roy, R. C. D. Brown, G. Pileio, and M. H. Levitt, The Journal of Chemical Physics **142**, 044506 (2015).
[24] S. S. Roy, J.-N. Dumez, G. Stevanato, B. Meier, J. T. Hill-Cousins, R. C. Brown, G. Pileio, and M. H. Levitt, Journal of Magnetic Resonance **250**, 25 (2015).
[25] P. K. Janert, *Data Analysis with Open Source Tools* (O'Reilly, 2010).
[26] C. Bengs and M. H. Levitt, Magnetic Resonance in Chemistry , 1 (2017).
[27] M. Carravetta, O. G. Johannessen, and M. H. Levitt, Physical Review Letters **92**, 153003 (2004).
[28] G. Pileio, Progress in Nuclear Magnetic Resonance Spectroscopy **56**, 217 (2016).
[29] M. H. Levitt, Annu. Rev. Phys. Chem. **63**, 89 (2012).
[30] G. Stevanato, J. T. Hill-Cousins, P. Håkansson, S. S. Roy, L. J. Brown, R. C. D. Brown, G. Pileio, and M. H. Levitt, Angewandte Chemie International Edition **54**, 3740 (2015).
[31] L. Olsen, O. Christiansen, L. Hemmingsen, S. P. A. Sauer, and K. V. Mikkelsen, The Journal of Chemical Physics **116**, 1424 (2002).
[32] G. Pileio, J. T. Hill-Cousins, S. Mitchell, I. Kuprov, L. J. Brown, R. C. D. Brown, and M. H. Levitt, Journal of the American Chemical Society **134**, 17494 (2012).
[33] A. B. Farimani, Y. Wu, and N. R. Aluru, Physical Chem-

istry Chemical Physics **15**, 17993 (2013).
[34] R. R. Ernst, G. Bodenhausen, and A. Wokaun, *Principles of Nuclear Magnetic Resonance in One and Two Dimensions* (Oxford University Press, 1987).
[35] J. Jeener, Advances in Magnetic Resonance **10**, 1 (1982).
[36] M. H. Levitt and L. Di Bari, Physical Review Letters **69**, 3124 (1992).
[37] T. Levante and R. Ernst, Chemical Physics Letters **241**, 73 (1995).